Sensors & Actuators: B. Chemical 426 (2025) 136959

Contents lists available at ScienceDirect

Sensors and Actuators: B. Chemical

journal homepage: www.elsevier.com/locate/snb

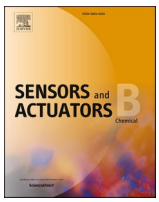

Accelerating hydrogen sensing with Pd-MOS capacitors using active controls of trapped charge

Nil Solà-Peñafiel [a], Gema López-Rodriguez [a], Pau Sindreu-Cladera [b], Eric Navarrete [c], Eduard Llobet [c], Juan Ramos-Castro [b], Isidro Martín [a], Xavier Manyosa [a,b], Sandra Bermejo [a], Manuel Domínguez-Pumar [a,b,*]

[a] Micro and Nano Technologies Group, Electronic Eng. Dept., Universitat Politècnica de Catalunya, Barcelona, Spain
[b] CTE-CRAE, Institute of Space Studies, IEEC, Castelldefels, Spain
[c] MiNOS Group, Universitat Rovira i Virgili, Tarragona, Spain

ARTICLE INFO

Keywords:
Trapped charge control
Sliding control
Pd-MOS capacitors
Hydrogen sensor
Sigma-delta modulation

ABSTRACT

Hydrogen monitoring with reliable, fast and cheap sensors is crucial to fully exploit the potential of this gas as an energy vector. One of the most appealing technologies for hydrogen sensing is based on MOS capacitors with palladium gate (Pd) made of nanoparticles, which acting as a catalyst for H_2 promotes its dissociation. The generated atoms are then injected into the dielectric shifting the C(V) curve. In this work, we show that the use of active controls of trapped charge in dielectrics can radically accelerate the response time of palladium MOS capacitors as H_2 sensors. The repeatability of the sensing is also improved, reducing significantly temporal drifts. The control strategy is based on second order sigma-delta modulation, implementing a discrete-time sliding mode control. Results show that the horizontal displacement of the C(V) curve of the capacitors can be cancelled out in real time by the application of voltage waveforms generated by the controls. Consequently, when exposed to hydrogen, a quasi-constant state operation of the capacitors is created, allowing a radical improvement of the time response as hydrogen sensors.

1. Introduction

In recent years, the use of hydrogen for industrial use and energy generation is rapidly increasing, becoming one of the most attractive candidates for a future energy carrier to replace fossil fuels [1–3]. Hydrogen detection in air is crucial for safety reasons, as the flammability and the detonation limits under atmospheric pressure are at 4 %, and at 18.3 %, respectively [4]. Moreover, since it is odorless, colorless and tasteless, humans cannot perceive leaks or emissions.

Traditional hydrogen sensing can be made using gas chromatographs, mass spectrometers or specific ionization gas pressure sensors [5]. However, these instruments are large, expensive and require high maintenance. In the last decades, there has been progress in developing miniaturized sensors for hydrogen detection based on different mechanisms: catalysis [6], electrochemistry [7], thermal conductivity [8], chemoresistance [9], work function [10], mechanical [11], optical [12] and acoustic [13]. In many of these different technologies, the use of palladium is key due to the high solubility of hydrogen in this material [14–16], being sensors based on MOS capacitors with Pd top electrodes one of the most appealing. Pd-gate FETs have been also fabricated, and even integrated in standard CMOS technology, although post process steps are usually required [17].

Numerous studies have investigated the chemical processes occurring within the palladium gate of MOS (Pd-MOS) devices [18,19]. The response of Pd-MOS capacitors exposed to hydrogen is typically associated with molecular hydrogen dissociation and formation of dipoles at the Pd gate-oxide interface, which leads to changes in the metal work function [20]. The presence of the dipole layer changes the flat band potential in the capacitor, inducing a voltage shift in the capacitance-voltage, C(V), characteristic for MOS capacitors, or a threshold voltage displacement in the case of MOSFETs. The dissociation of the hydrogen molecule occurs due to the catalytic nature of palladium, and the generation of the dipole layer at the Pd gate-oxide interface is generally considered a fully reversible and fast process [20]. On the other hand, other slower mechanisms with a wide distribution of time constants have been proposed behind the shifts of the C

* Correspondence to: UPC-Campus Nord, Jordi Girona, 1-3. 08034, Barcelona, Spain
E-mail address: manuel.dominguez@upc.edu (M. Domínguez-Pumar).

https://doi.org/10.1016/j.snb.2024.136959
Received 26 July 2024; Received in revised form 23 October 2024; Accepted 15 November 2024
Available online 29 November 2024

(V) characteristic:

a) the field dependent movement of protons in the silicon oxide layer [20,21], as hydrogen travels in the oxide as H^+, which is more stable than neutral hydrogen atoms [22,23].
b) the formation of interfacial states at the Si-SiO_2 interface, resulting in charged dangling bonds. The steps in this process are: dissociation of the hydrogen molecules on the Pd-surface, adsorption of the dissociated atoms on the metal surface, diffusion of the atoms to the Pd-SiO_2 interface, diffusion/tunneling through the oxide layer leading to hydrogen accumulation at the Si-SiO_2 interface, and finally formation of positively charged dangling bonds due to the reaction of protons with Si-H complexes, through the following reaction [21,22,24]:

$$SiH + H^+ \rightarrow D^+ + H_2 \quad (1)$$

Other mechanisms capable of generating horizontal shifts of the C(V) characteristic of MOS capacitors come from the generation of trapped charge at the silicon-oxide interface, or in the oxide, due to the long-term application of stress voltages. These effects have become an important reliability issue for many years in MOS transistors, and are known as Bias Temperature Instability (BTI), both for positive (PBTI) and negative bias (NBTI). Under continuous DC bias stress, by positive or negative voltages, on the gate of MOS transistors and capacitors, charge trapping occurs in the oxide, becoming one of the main aging mechanisms in MOS transistors [25,26]. Hydrogen plays an important role in BTI, as shown for example in the Gate-Sided Hydrogen Release (GSHR) model [26]. During BTI stress, H tends to migrate from the oxide to the Si-SiO_2 interface. Once the H reaches this interface, it can become trapped to create new donor-like oxide defects [27–29], or break Si-H bonds directly at the gate-channel interface to create P_b-centers [30]. Furthermore, this charge trapping is typically accelerated under thermal stress.

In parallel, active control loops have been designed allowing to control trapped charge in oxides by applying appropriate gate bias voltages, generated by a closed feedback loop. The controls, initially introduced in reference [31], have found successful implementation in electrostatic microelectromechanical systems (MEMS) [32–34] and MOS capacitors [35–37]. Additionally, it has been possible to implement the first active compensation of trapped charge generated by ionizing radiation [36,38,39].

The objective in this paper is to apply charge trapping control methods to a Pd-MOS capacitors while being exposed to hydrogen. This exposure would naturally generate horizontal displacements of the C(V) characteristic of the MOS capacitor. The objective of the control is to avoid these displacements by generating the required bias voltages. Since now the C(V) will be located at a constant position, the new output signal of the sensor will be the average bias voltage generated by the control, i.e., the signal related to the control action. This type of active compensation can be seen as an example of what may be called *quasi-static state operation of sensors*: active controls try to freeze the state of the sensors when exposed to the external magnitude to measure, which, from the point of view of the control, can be considered as a disturbance. Since the state of the sensor is almost constant, the control action is then the new output of the system. These types of controls have been implemented in wind sensors for Mars in three NASA missions by implementing Constant Temperature Operation [40], in thermopiles [41] and in gas sensors based on metal oxides [42]. By operating under these conditions, it is possible to radically change the natural temporal response of the sensors. Consequently, the novel approach reported hereby paves the way to fast, cheap and reliable hydrogen sensors.

2. Control design

As it has been mentioned, adsorption of hydrogen in Pd capacitors triggers displacements of the C(V) curve of the device. The objective of the trapped charge control is to 'freeze' the C(V) curve compensating the effects of hydrogen adsorption/desorption by adapting the average bias voltage. This means that the control will apply voltage waveforms to the capacitor with two objectives: compensating the hydrogen-induced shifts by changing the actuation voltages and periodically monitoring the shift in the C(V) curve.

The implemented control is based on 1-bit sigma-delta modulation. The controller uses a feedback loop to control the displacement of the C (V) curve. It does so by keeping constant the capacitance of the device, measured at a given measurement reference voltage (V_{meas}). The control tries to enforce the condition $C[V_{meas}](nT_S) = C_{th}$, for all sampling times nT_S where n is a natural number and T_s is the sampling period. In order to keep the C(V) stable we will implement a sliding mode control, using time discretization. We use two waveforms that have opposite effects on the horizontal movement of the curves: one displacing the C(V) curve to the left, and the other to the right. As it is explained in the next subsection, the waveforms have been designed to generate the aforementioned shift (by having different average bias voltage), while at the same time being able to periodically monitor the bias voltage so that the capacitance is measured at a constant reference voltage (V_{meas}). This can be understood as a fast-slow process. The fast components allow switching the bias voltage for a short time interval in order to compare the position of the current C(V) curve with regard to a reference; while the slow process consists of the displacement generated by the bias voltage for most part of the duration of the waveforms.

2.1. Waveform design

One of two waveforms, referred to as BIT1 and BIT0, will be applied to the capacitance (see Fig. 1-Left), during a certain sampling period, $nT_s \leq t \leq (n+1)T_s$, depending on the previous readings of the capacitance: $C[V_{meas}](kTS)$ for $k \leq n$. The specific dependence is determined by the specific topology of the controller used (in this work first or second order sigma-delta modulator). In the case of first order topology, and as an example for a better understanding of how the control works, the following logic would apply:

$$\begin{cases} \text{if } C[V_{meas}](nT_S) > C_{th}, & \text{BIT0 is applied on the next period} \\ \text{if } C[V_{meas}](nT_S) < C_{th}, & \text{BIT1 is applied on the next period} \end{cases}$$

The logic behind this first order control is that the waveform applied during the next clock cycle must try to counteract any shift from the condition $C[V_{meas}](kTS) = C_{th}$. There is more information on this controller in the Appendix.

This type of control actions will generate an output binary *bitstream* consisting of the sequence of BITs generated, i.e., $b(n) = 1$, when a BIT1 is applied during the time interval $nT_S \leq t \leq (n+1)T_S$; and $b(n) = 0$ when a BIT0 is applied during the same time interval.

The BIT0 and BIT1 signals are composed of two parts. The first part is designed to change the average bias voltage on the device, whereas the second part is designed to periodically monitor the position of the C(V) by implementing a fast voltage switching to measure at the constant reference voltage, V_{meas}:

- During the first part of the waveform, the T_{bias} time interval, a V_{low} (in BIT1) or V_{high} (in BIT0) bias voltage is applied. The objective of this part of the waveform is to change the average bias voltage in the device, and therefore sustain the slow dynamics process related to the horizontal shifts of the C(V) curve. We will see later in Section 5 that the continuous application of a low voltage tends to shift in the C (V) to higher voltages, whereas the application of a high voltage shifts the C(V) to more negative voltages, as can be observed in Fig. 1-Right.
- The second part of the waveform corresponds to the time interval where the measurement voltage V_{meas} is applied, denoted as T_r, to

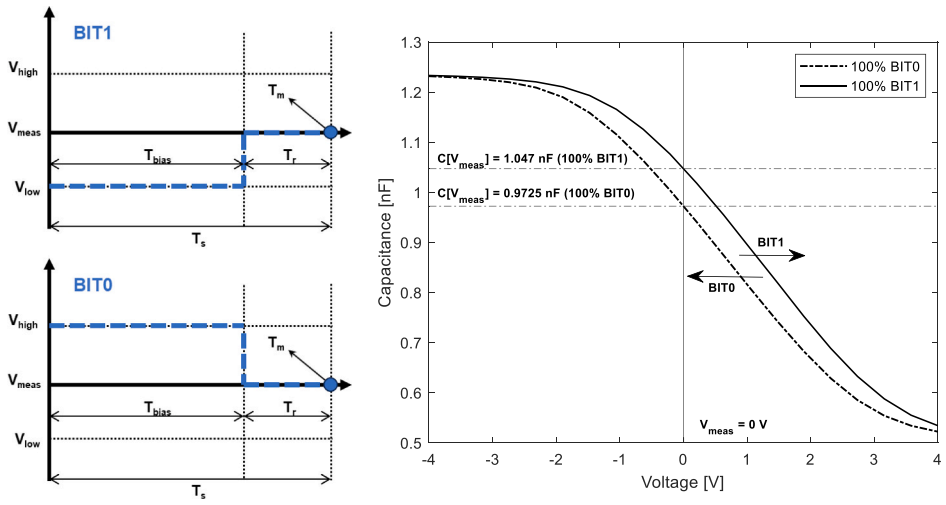

Fig. 1. (Left) Sigma-delta bias voltage waveforms. During the first-time interval, T_{bias}, V_{low} and V_{high} are applied to generate sustained displacements of the C(V) curve. During the second interval, T_r, voltage is kept constant at V_{meas} and the capacitance of the Pd-MOS is measured (at instant T_m). (Right) Example of the C(V) displacement when BIT1s and BIT0s are applied for a long time ($V_{meas} = 0$ V, $T_r = 75$ ms, $T_s = 150$ ms, T = 90°C. $V_{high} = 0$ V, $V_{low} = -8$ V, flow of synthetic air = 300 mL/min). By looking at the C(V) curves of the right it is possible to see that, at a fixed voltage (for example $V_{meas} = 0$ V) the measured capacitance increases with BIT1 while it decreases with BIT0.

monitor the capacitance value, which is measured at instant T_m. This capacitance value is continuously used in the control feedback loop. The total duration of the waveform is the sampling period, T_s. The objective of the fast switching inside the waveform, during T_r, is to monitor the value of the capacitance, measured at constant voltage, without significantly altering the position of the C(V) curve.

The new output signal using this control will no longer be the capacitance measured at V_{meas}, as it would be in the case of using the hydrogen sensor in open-loop. Instead, it will be the average number of BIT1s in the bitstream, calculated with a moving window (i.e., by averaging the last N bits):

$$O(n) = \frac{1}{N}\sum_{k=1}^{N} b(n-k) \tag{2}$$

This filtered bitstream, O(n), can be seen as the control action determined by the feedback loop to keep constant the C(V) of the device. The range of this new output will be between 0 % (all BIT0) and 100 % (all BIT1). A more intuitive way to understand the new control output is to see it as the average bias voltage applied by the control to the circuit during N number of cycles, i.e., a moving average of the applied voltage:

$$V_{\Sigma\Delta}(n) = \frac{1}{N}\sum_{k=1}^{N} V_{bias}(n-k) \tag{3}$$

Where V_{bias} is the bias voltage applied during the T_{bias} time interval at each BIT waveform (which will be V_{low} or V_{high}). In a typical application, the filtered bitstream output is decimated by N so that consecutive samples of the output signal are independent.

2.2. Control loop

The intuition behind the control is that the BIT0 and BIT1 waveforms must have opposite influence on the magnitude to be controlled. At each sampling time, the control calculates the difference between the actual value of the magnitude to control, $C[V_{meas}](nT_S)$, with the desired value, C_{th}. This difference is fed into the integrator, in order to implement a second order modulator topology.

Although it is a widely used architecture in control systems, first order sigma-delta can present plateaus in the bitstream (see the Appendix). In our case, this effect appears when the magnitude of the sampling time is comparable or greater than the shortest time constant of the MOS charging and discharging processes [34,37,43]. When this occurs, the control may provide a constant bitstream pattern at the output, in which the system is effectively in open-loop configuration. In order to avoid the problems of first order modulators, a second order sigma-delta modulator has been implemented (see Fig. 2). This modulator includes an additional integrator before the sign detector [37,42].

3. Pd-MOS capacitor fabrication process

The fabrication process for the capacitors starts with an RCA cleaning process of a 4" p-type c-Si wafer, with a resistivity of 3Ωcm. Subsequently, a thermal oxidation is carried out at 1000°C for 60 minutes in O_2, resulting in a measured thickness of 48 nm as determined by ellipsometry. The silicon oxide at the rear side is etched with NH_4/HF for 1:30 minutes, protecting the front side with photoresist as a prior safeguard. After removing the photoresist, the wafer is placed in a magnetron sputtering to deposit Titanium and Platinum creating the bottom contact, resulting in a combined thickness of 430 nm. At the end of the process the capacitors were cut into squares of 6 mm× 6 mm.

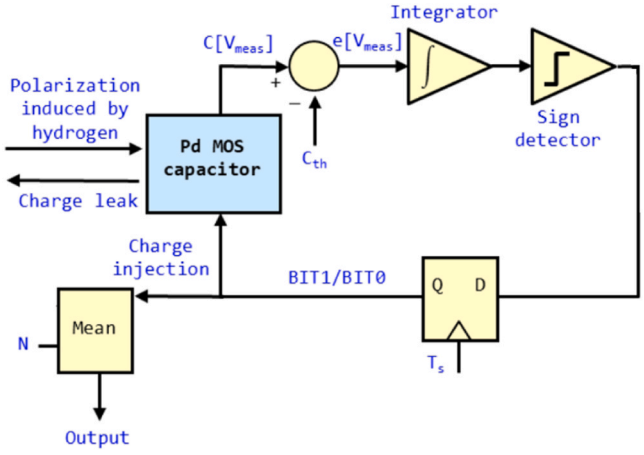

Fig. 2. Second order sigma-delta control block diagram. The feedback loop is such that: $b(n) = sgn(I_n)$, where $I_n = I_{n-1} + e[V_m](n)$, with $e[V_m](n) = C[V_{meas}](nT_S) - C_{th}$.

The top electrode of the capacitance is made of Pd nanoparticles (see Fig. 3), nanopowder with particle size < 25 nm from Sigma-Aldrich CAS: 7440–05–3. The objective of using this type of nanoparticles is to ensure a uniform deposition and optimal material characteristics. Initially, 10 mg of Pd-nanoparticles were weighed in an analytical weighing scale and transferred to an agate mortar. Subsequently, between 10 and 20 µl of 1,2-propanediol were added to achieve a homogeneously viscous mixture through meticulous manual stirring. The mixture viscosity is a key parameter to ensure the consistent material delivery during the drop-coating step. Then, 2 µl aliquots of the resultant mixture were carefully pipetted and deposited onto the silicon oxide substrate. This deposition step was repeated 2–4 times, depending on the desired thickness and uniformity of the nanolayer, ensuring consistent coverage across the substrate, but preventing the droplets from reaching the edges. Following the deposition, the samples were dried in an oven at 70 °C overnight to remove any residual solvent gently.

Fig. 4 shows a photograph of one of the devices, and Fig. 5 shows the Pd nanoparticles FE-SEM microphotographs.

The chemical composition of the samples, the layer morphology and the crystallinity were studied. The microscopes used were a field emission scanning electron microscope (FE-SEM), a Scios 2 from Thermo Fisher Scientific was used to obtain the scanning electron images. The high-resolution images were acquired using the in-column detectors applying a 5 kV accelerating voltage. For the EDX analysis a Thermo Fisher EDX detector with 100 mm^2 size was operated. The EDX data were obtained using PathFinder software. A high-resolution transmission electron microscope (HR-TEM), a JEOL F200 TEM ColdFEG operated at 200 kV was used for the transmission electron microscopy characterization. TEM images were acquired with a Gatan OneView camera, a CMOS-based and optical fibre-coupled detector of 4096 × 4096 pixels. Gatan Digital Micrograph program was used to process the TEM images. STEM images (1024 × 1024 pixels) were recorded from the JEOL bright-field (BF) and high-angle annular dark-field (HAADF) detectors using the Gatan DigiScan3 scanning unit with a camera length of 250 mm. Samples were inserted in a JEOL beryllium double-tilt holder for energy dispersive x-ray spectroscopy (EDS). STEM-EDS mapping was recorded from an EDS Centurio detector (silicon drift) with an effective area of 100 mm^2 and 133 eV of energy resolution. STEM-EDS maps (512 × 512 pixels) were processed with the JEOL Analysis software.

In Fig. 5 the FE-SEM imaging of the surface is shown together with a close look into its morphology. The mild thermal treatment does not fully remove the remnants from the organic solvent, and therefore spherical carbon particles are present in the surface. The nanoparticles have clustered into a compact yet porous palladium layer. The porosity is attributed to the evaporation of the organic solvent all along the layer during the mild temperature treatment. Furthermore, there are no signs of nanoparticle sintering either suggesting that the particles are aggregated but not amalgamated.

HR-TEM analysis revealed the presence of aggregated nanoparticle clusters. The presence of spherical carbon particles resulting from the non-complete removal of the solvent used to synthesize the layer can be observed. Despite the presence of carbon, the Pd nanoparticles have kept

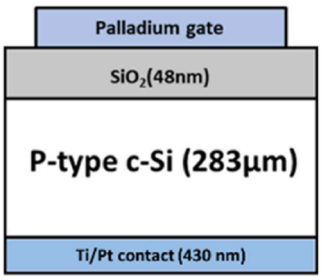

Fig. 3. Cross section of the hydrogen-sensitive Pd-MOS capacitors.

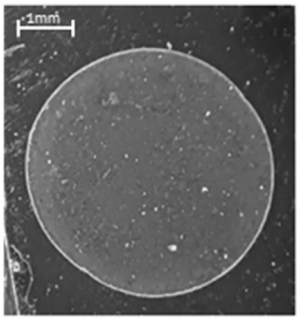

Fig. 4. Hydrogen-sensitive Pd-MOS capacitor fabricated.

their structure, and they form agglomerates. In Fig. 6 the HR-TEM images from the Pd nanoparticles are shown and, the interplanar distance has been measured to a value of 0.275 nm. According to the literature [44,45], the actual spacing of the Pd atoms on the (111) surface is 0.275 nm vs the Pd-Pd nearest distance in PdO being 0.305 nm, thus confirming that the material present in the sample is metallic palladium.

An elemental mapping of both layers was carried out. In the energy-dispersive X-ray spectroscopy (EDS) map, the palladium (Pd) is indicated by the blue color and the oxygen (O) is indicated by the red color, see Fig. 7. The presence of oxygen in the sample, despite it may suggest the presence of a palladium oxide component, is mainly attributed to adsorbed oxygen at the nanoparticle surface, as the HR-TEM results indicate the presence of metallic Pd.

4. Experimental setup

In order to be able to measure the capacitor capacitance, a mechanical device has been manufactured which allows to change the sample in a simple way and without damaging the palladium gate. The schematic of this mechanical system, and detailed pictures, can be seen in Fig. 8.

Fig. 9 gives a schematic representation of the experimental setup used. The MOS capacitor is placed inside a 4 mL dead volume gas chamber, connected to two bottles: one of pure synthetic air and another one with 1000 ppm of hydrogen in pure synthetic air. The chamber, and consequently the Pd-MOS devices, is placed inside an oven, to be able to measure at different temperatures. The hydrogen concentration is modified using mass flow meters (MFC), which have been programmed to controlled concentrations, while keeping a constant flow in the system. The hydrogen bottle used contains 0.1 % (1000 ppm) hydrogen and 20.88 % oxygen. The remainder is nitrogen. The pure synthetic air bottle contains 21 % oxygen and 79 % nitrogen (± 0.1 %) and purity of P > 99.999 %. The two bottles are supplied by Nippon Gases.

A precision LCR meter Keysight E4980A is used to generate the control voltage waveforms applied to the capacitor, and to measure the device capacitance. The typical deviation of the measurement, in the 0.5 nF – 1.5 nF range is below 6 fF. The measured data is then transmitted to a computer for analysis and processing. The determination of the waveform to be generated in the next cycle is carried out by real-time software running on a PC.

The I-V characteristic of one of the devices fabricated can be seen in Fig. 10

5. Experimental results

To understand the devices and how to optimize the voltage at which the capacitance must be measured, it is necessary to monitor the C(V) curves. To do this, an AC signal of 200 kHz and $V_{pp} = 2$ V has been generated with the LCR meter. The measuring frequency has been selected in order to have a good signal-to-noise ratio (for example avoiding very high frequencies, where interferences and cabling can

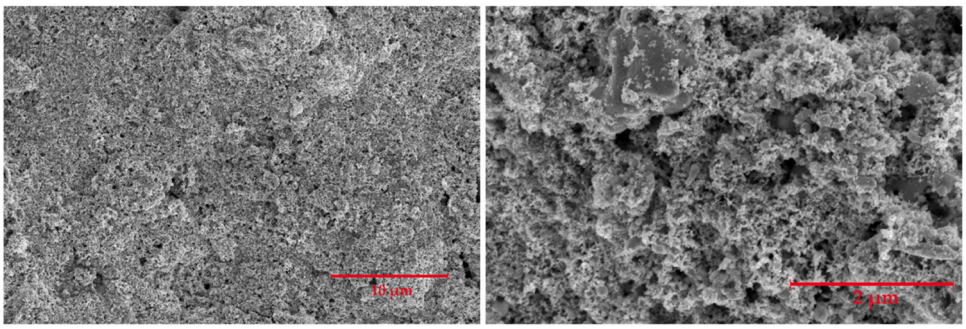

Fig. 5. FE-SEM micrographs surface for Pd-nanolayers (left panel) and a closer look into the surface (right panel).

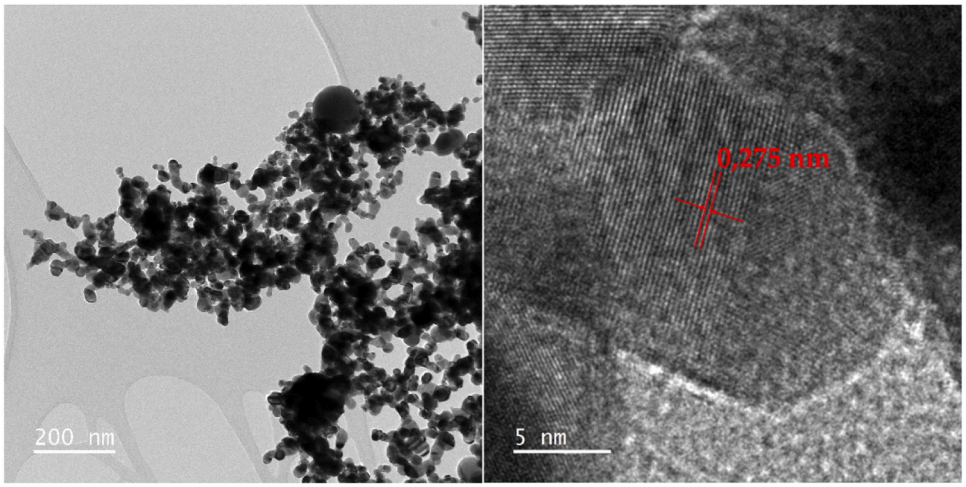

Fig. 6. HR-TEM images. Detail of the Pd nanoparticles with some larger carbon spherical nanoparticles can be seen (left), close-up to the interplanar distance and the nanoparticles crystallinity (right).

easily become critical), while keeping a high frequency in order not to have long measurement times, which would limit the maximum sampling frequency used in the control loop. As an example, Fig. 11 shows how the C(V) curves of one device are displaced after exposure to 100 ppm of hydrogen for 6 minutes, for 2 kHz and 20 kHz. As can be observed, the sensitivity to hydrogen in both cases is similar. This coincides with results in the literature, [21] indicating that the use of low frequencies may increase sensitivity at high concentrations, but not in the case of low concentrations (< 1500 ppm).

The optimal voltage to measure the capacitance (V_{meas}) is the one where the difference in capacitance is maximum when the C(V) is shifted along the voltage axis under the presence of hydrogen. This optimal V_{meas} will coincide with the point of maximum slope of the curve.

Furthermore, in order to have an effective control of the capacitance, the C(V) curves of the Pd-MOS device must be sensitive to both hydrogen concentration and bias voltage changes within the same magnitude range. To demonstrate this point, a series of experiments have been carried out with one of the fabricated Pd-MOS devices. In Fig. 12, we show the time evolution of the capacitance measured at constant voltage (V_{meas}) of the Pd-MOS structure when different bias voltages are applied to the gate (i.e. the voltage applied during the T_{bias} interval is swept during the experiment), and the capacitance is periodically measured at constant bias V_{meas}= 0 V. As can be seen, for increasingly positive bias voltages, the capacitance becomes smaller (indicating a shift of the C(V) curve to lower voltages), and for increasingly negative voltages the capacitance becomes larger (indicating a shift of the C(V) curve to higher voltages).

The voltage pair, V_{high} and V_{low}, chosen depends on two factors. The greater the difference between the high and low voltages, the wider the range of hydrogen concentrations the sensor can cover, but this will also reduce its sensitivity. Another factor to consider is the operating region where capacitance control is desired. This is important because controlling the C(V) in different regions gives rise to different behaviors. In our devices, as we have chosen the voltage where the C(V) slope is maximum, we maintain the Pd-MOS under depletion/weak inversion conditions.

As can be seen in Fig. 12, the ability of changing the capacitance by applying a bias voltage to the gate is confirmed. Fig. 13 illustrates the response of one of the fabricated devices when H_2 are applied. As illustrated, the C(V) curves exhibit a shift to the left upon the introduction of hydrogen and a corresponding rightward shift upon its removal. The experiment consists of exposing the device to 100 ppm of H_2 for 5 minutes (Fig. 13, top-left), after which the hydrogen is removed and pure synthetic air is injected, for 5 minutes more (Fig. 13, top-right). Fig. 13 bottom, shows the time progression of the capacit*ance measured at* V_{meas}.

Combining both experiments, it can be concluded that the presence of hydrogen, or the application of V_{high} polarization voltages (BIT0), induces a shift to lower voltages of the C(V) curve resulting in lower capacitance values at V_{meas}; whereas removing hydrogen, or applying V_{low} polarization voltages (BIT1), results in a rightward shift (see Fig. 14). This behavior may enable the control of the capacitance by a closed-loop.

After this characterization, an experiment has been carried out consisting of a 30-minute pulse train where the hydrogen concentration has been gradually increased from 50 ppm to 500 ppm. To verify the stability of the sensor, the experiment has been repeated four times

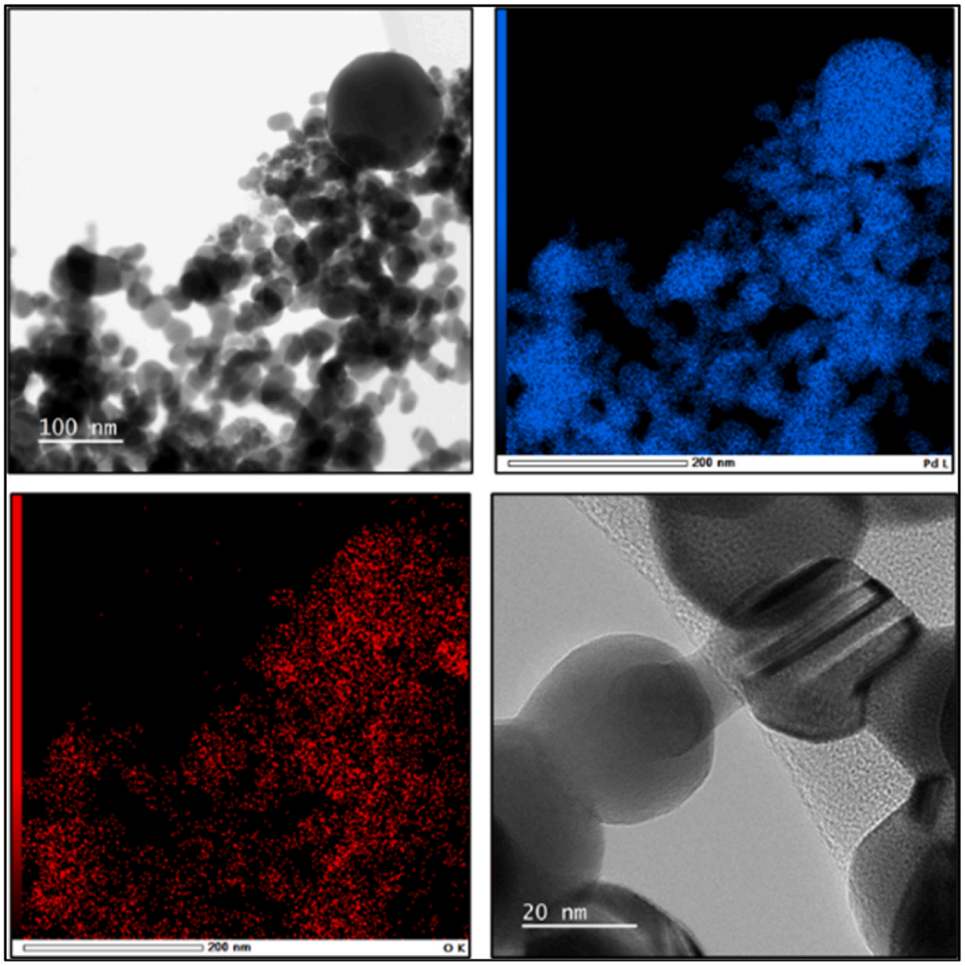

Fig. 7. Nanoparticles and chemical mapping (energy-dispersive X-ray spectroscopy (EDS) map). Elemental mapping colors correspond to palladium in blue and oxygen in red.

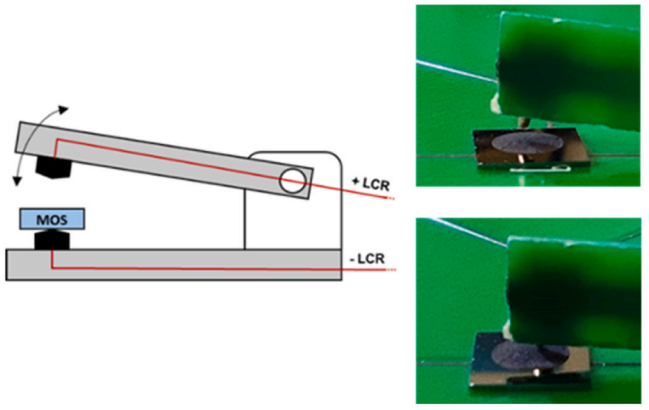

Fig. 8. (Left) Schematic of the mechanism fabricated for contacting the MOS capacitors. (Right) Detail of the mechanism, in the up-position (top), and down-position (bottom).

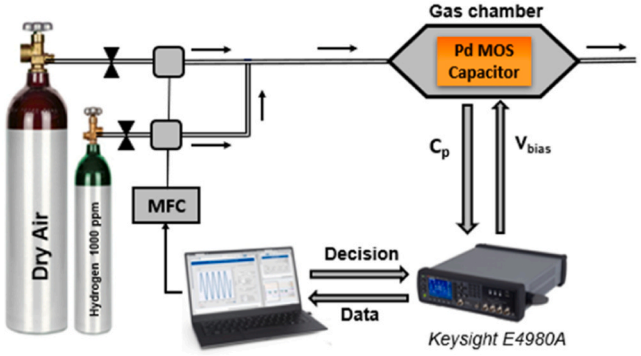

Fig. 9. Description of the experimental setup.

consecutively. Between each hydrogen concentration peak, the sensor was allowed to stabilize in pure synthetic air to analyze both the response time and behavior in hydrogen absorption and desorption. As in previous cases, the experiment was conducted in both open-loop and closed-loop control modes. For the open-loop measurement, a fixed percentage of the bitstream is applied (in this case 10 %), to avoid continuous application of the same bias voltage, which tends to increase bias-induced drifts. The results can be seen in Fig. 15.

The use of the closed-loop control clearly improves the sensor performance. In particular, one of the main advantages is the repeatability of the measurements. In other words, the different H_2 concentrations lead to very similar output values in all four repetitions (Fig. 15 bottom) while the open-loop case (Fig. 15 top) shows a drift that hinders the H_2 concentration measurement directly from the capacitance value. This improvement is based on the fast and systematic sensor recovery in H_2 desorption process, i.e. after stop being exposed to hydrogen the sensor output comes to the initial value, whereas in the open-loop case this does not happen, generating drift. Additionally, and focusing on the H_2

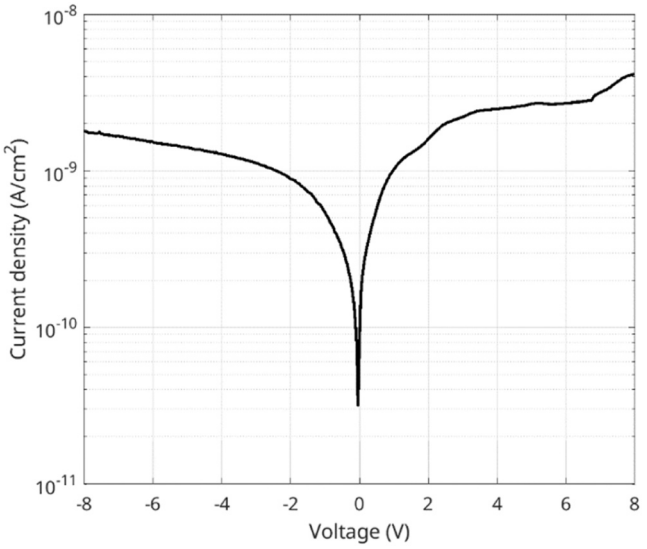

Fig. 10. I-V characteristic of one of the fabricated devices.

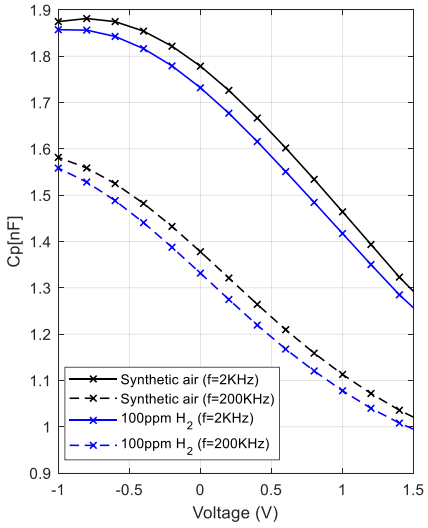

Fig. 11. C(V) characteristics of a device measured in synthetic air, and after 6 minutes of exposure to 100 ppm of hydrogen, measured at two different frequencies (2 kHz, and 200 kHz).

adsorption, although the response times are similar, the sensitivity of the controlled sensor is much higher. This can be seen in the relative differences of the final sensor response values to the different H_2 concentrations: under closed-loop control, the relative differences in response between different concentrations are higher than under open-loop operation.

One of the main limitations of the controlled measurement is that the detection range is limited. This means that the control output can reach saturation if the applied hydrogen concentration is able to shift the C(V) more than the constant application of BIT1 or BIT0 can. When this happens, controllability is lost. This situation is illustrated in Fig. 16. The experiment described is a continuation of the one presented in Fig. 15, but with an extension of the concentration range up to 1000 ppm. As can be seen, when this H_2 concentration is applied, the output saturates to 100 %. At this point, the capacitance is no longer controlled around the threshold value and its behavior changes to an open loop operation. This is evident from the average measured capacitance represented in black in Fig. 16, Bottom. However, more importantly, the control can recover from this situation and it works correctly again when concentrations within its sensing range are reapplied. In addition to recovering, the response time of the saturation output is still much faster with the closed-loop control than when in open-loop.

Another important factor to take into account for the controlled sensors is the choice of the threshold capacitance, C_{th}. In all previous measurements, the device was initially stabilized with synthetic air and a bitstream sequence of 10 % was programmed. As a result, the threshold capacitance is the one measured under these circumstances with $V_{meas} = 0$ V. In this way, when applying hydrogen pulses, almost the entire dynamic range is available to observe the sensor response. In Fig. 17, we explore the effect of changing the threshold capacitance while keeping the same H_2 concentration (100 ppm). As can be observed, the sensitivity of the sensor significantly changes being higher for higher threshold capacitance. It must be mentioned that abrupt step down or small exponential decays observed in Fig. 17 correspond to the control response to the threshold capacitance change in real time during the experiment.

As has been mentioned before, the selection of the control parameters must take into account the desired sensing range for the application. It must be pointed out that the control works well; avoiding saturation, in the low concentration regime, indicating that this type of controls may help in the detection of gas leaks.

6. Discussion and analysis

As it has been described in the previous sections, a shift in the C(V) curves can be induced by applying a low (BIT1) or high (BIT0) voltage to

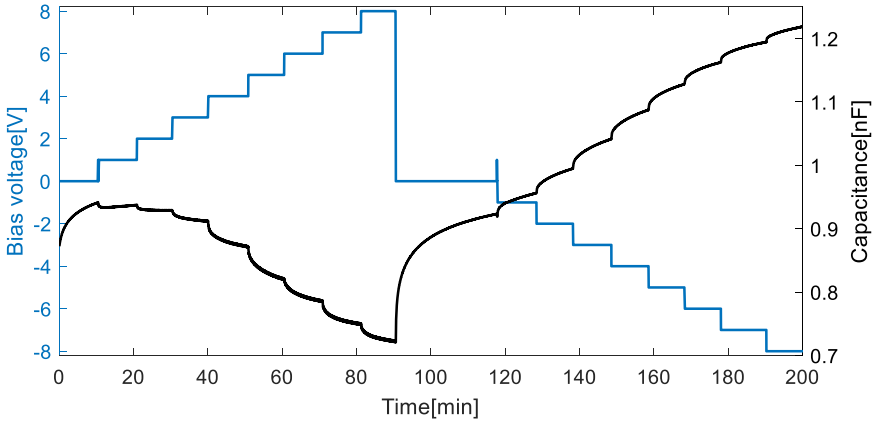

Fig. 12. Capacitance behavior due to different bias voltage. Measurement done under a constant pure synthetic air flow of 300 mL/min. ($V_{meas} = 0$ V, $T_r = 75$ ms, $T_s = 150$ ms, $T = 90$°C. The bias voltage applied at each waveform is swept during the experiment, and it is indicated by the blue curve).

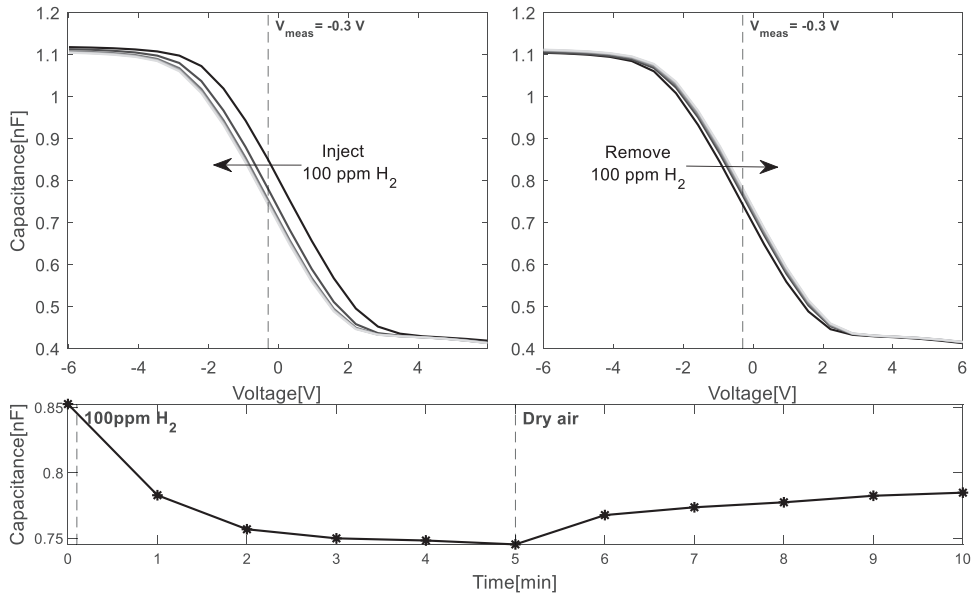

Fig. 13. *Behavior due to different hydrogen concentrations. Top-left: C(V) evolution when the sensor is exposed to 100 ppm of hydrogen. Top-right: C(V) evolution after hydrogen removal. Bottom: capacitance evolution throughout the experiment. For the BIT waveforms used, the parameters are: V_{meas} = -0.3 V, T_r = 75 ms, T_s = 150 ms, T = 90°C. The bias voltage applied at each waveform is constant = 0 V. Total flow during the measurement = 300 mL/min.*

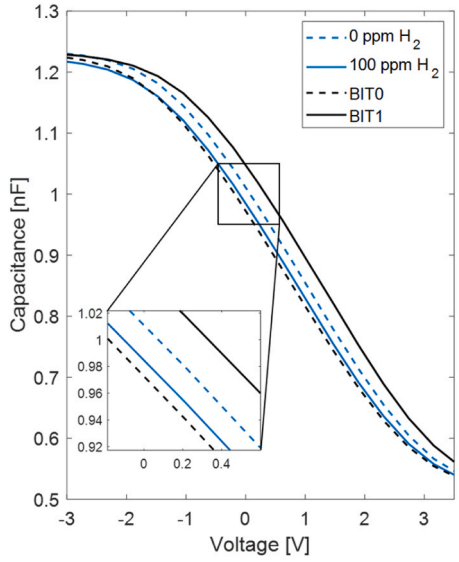

Fig. 14. C(V) curves of Pd-MOS device when the capacitor is subjected to different conditions. The blue curves result from exposing the device to 100 ppm of hydrogen (discontinuous line) and pure synthetic air (continuous line). The Bitstream percentage for these curves has been kept constant at 50 % (constant alternation of BIT0 and BIT1). The black curves result from continuously applying BIT1, i.e., Bitstream= 100 % (discontinuous line), and BIT0, i.e., Bitstream= 0 % (continuous line). The C(V) curves of hydrogen changes are within the limits marked by the control saturation represented by the black lines, indicating that a measurement under closed-loop without saturations is possible. For the BIT waveforms used, the parameters are: V_{meas} = 0 V, T_r = 75 ms, T_s = 150 ms, T = 90°C. V_{high} = 0 V, V_{low} = -8 V. Total flow during the measurement = 300 mL/min.

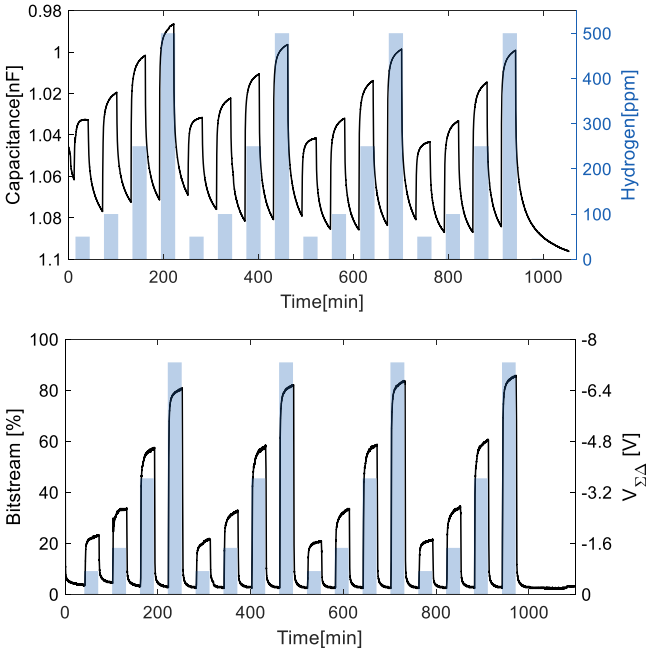

Fig. 15. Comparison between open-loop, with a constant bitstream with 10 % BIT1s (top), and closed-loop (bottom) measurements. Experiment consisting on a 30-minute pulse train where the hydrogen concentration has been gradually increased from 50 ppm to 500 ppm. For the BIT waveforms, the parameters are: V_{meas} = 0 V, T_r = 75 ms, T_s = 150 ms, T = 90°C. V_{high} = 0 V, V_{low} = -8 V. Total flow during the measurement = 300 mL/min.

the gate of the Pd-MOS capacitors. For example, the continuous application of a low bias voltage, V_{low}, increases the capacitance value of the sample at V_{meas}, i.e. it shifts the C(V) curve to positive voltages; while the continuous application of V_{high} results in the opposite shift. Interestingly, this particular behavior can enlighten the possible physical mechanism behind it.

For a P-type substrate, like the ones used in this work, V_{high} leads to the attraction of electrons to the SiO_2/c-Si surface due to the induction of an electric field in the semiconductor. If part of these electrons gets trapped at the SiO_2/c-Si interface (for example by filling interface states or getting trapped in the first monolayers of the SiO_2) an additional negative charge in the oxide is created shielding the effect of the voltage at the gate. The resulting effect is an increase in the flat-band voltage, because now higher voltages are needed to induce the same electric

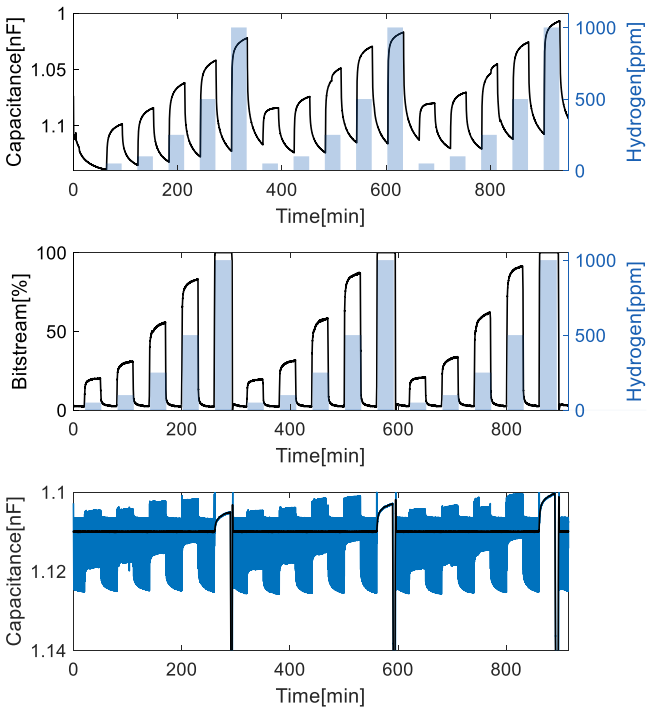

Fig. 16. Same experiment as in Fig. 15, but increasing the hydrogen concentration up to 1000 ppm. In the top figure, the open-loop response. In the middle, the control output bitstream is shown. In the bottom graph, the capacitance measurement at the instant T_m of each BIT pulse (in blue) and its mean (in black) are shown. Open-loop measurement has been performed at a constant bit stream of 50 %. For the BIT waveforms, the parameters are: V_{meas} = 0 V, T_r = 75 ms, T_s = 150 ms, T = 90°C. V_{high} = 0 V, V_{low} = -8 V. Total flow during the measurement = 300 mL/min.

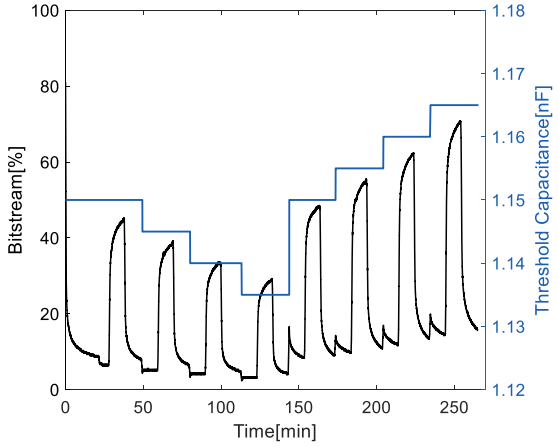

Fig. 17. Experiment performed to observe the response of the sensor when subjected to 100 ppm hydrogen pulses, while simultaneously adjusting the threshold capacitance of the control (blue line). For the BIT waveforms, the parameters are: V_{meas} = 0 V, T_r = 75 ms, T_s = 150 ms, T = 90°C. V_{high} = 0 V, V_{low} = -8 V. Total flow during the measurement = 300 mL/min.

field, i.e. band bending, at the c-Si. Consequently, a C(V) curve measured after applying V_{high} for a certain time would shift the C(V) to higher voltages. Alternatively, if we apply a low voltage (V_{low}) the holes are the ones attracted to the surface leading to positive charge trapped in the SiO_2/c-Si interface and, thus, a negative shift in the C(V) curve is expected.

Notice that the experimental behavior of our devices described above is the other way round. This means that the dominant mechanism behind the capacitance control cannot be related to changes in the charge trapped at the SiO_2/c-Si interface and, thus, the only possibility is linked to changes at the Pd/SiO_2 interface.

In the literature [20], the shift of C(V) curves of Pd-MOS capacitors under the presence of H_2 has been mainly justified by the appearance of dipoles close to the Pd/SiO_2 surface. The idea is that H^+ ions reach that interface by diffusing through the Pd and they penetrate into the SiO_2. However, the diffusion of H^+ into the SiO_2 is drastically slowed down by the formation of the dipole together with the image charge that appears at the Pd surface. As a consequence, the H^+ ions will be in the first monolayers of the SiO_2 statistically distributed and they are the responsible for the slow drift of the capacitance under the presence of significant H_2 content [20].

From the point of view of the bias voltages, the application of V_{high} (BIT0) at the gate results in the drift of more H^+ into the SiO_2 and the repealing to deeper SiO_2 monolayers of those already there. As a consequence, a higher positive charge at the SiO_2 (or an apparent reduction of the metal workfunction due to the dipole presence) is obtained leading to a C(V) curve drifted to negative values, i.e. lower capacitance values will be measured. On the other hand, when V_{low} (BIT1) is applied H^+ ions are attracted to the Pd surface and they can even be desorbed through the Pd. As a result, the C(V) curve is shifted to positive voltages and the measured capacitance increases.

This may also explain the change in the time response of the sensors. When the capacitance is exposed to H_2, the introduction and release of H^+ close to the Pd/SiO_2 interface would naturally tend to increase the concentration of H^+ in the first monolayers of the SiO_2, with the associated slow drift in the C(V) curve, once the protons start drifting inside the oxide. The control, with its objective of maintaining a constant capacitance, increases the average number of BIT1 waveforms, thus lowering the average bias voltage in the gate. The application of a lower bias voltage tends to counteract the drift into the oxide of the protons, by keeping them near or at the Pd/SiO_2 interface, or even removing them towards the Pd electrode. This means that the control tends to keep constant the state of the sensor (the concentration of protons inside the oxide), and therefore compensates the external disturbance created by exposing the capacitance to H_2.

Furthermore, this may also help to explain the full recovery of the sensors to their initial states when the ambient H_2 is removed compared to the open-loop case. Under uncontrolled constant bias voltage, the concentration of protons inside the oxide would change as a result of exposing the capacitance to different H_2 concentrations. This process would slowly drift the C(V) of the device to negative voltages. However, if the capacitance is being controlled, the control limits the introduction of protons inside the oxide to shallower SiO_2 layers by applying a more negative average bias voltage. As a consequence, when the exposure to H_2 ceases, no significant internal drift of the protons towards the gate needs to happen. The absence of this proton drift means that control action (the output signal) enables a much faster transition than in the open-loop (constant bias voltage) situation.

Finally, the capability of controlling the capacitance, even in the absence of H_2, could be related to the PBTI and NBTI effect in MOSFET transistors where the hydrogen is transported through the SiO_2 depending on the applied gate voltage [25,26]. As it is mentioned in the literature, this transport is highly dependent on the device temperature, as we have already seen in our sensors, which significantly reduce their sensitivity when measured at room temperature.

7. Conclusions

Our experimental findings demonstrate the efficacy of employing sliding mode control to enhance the performance of Pd-MOS capacitors for hydrogen sensing. The use of a trapped charge control consistently exhibits faster response times (with recovery times reduced by at least a factor 10) and better stability and reproducibility compared to conventional methods. The implementation of second order sigma-delta

modulation further improves control system stability, addressing limitations observed in first order modulation. These results highlight the potential of Pd-MOS capacitors as reliable and cost-effective hydrogen sensors, with implications for enhancing safety in industries utilizing hydrogen. Future work will focus on modeling the charge dynamics inside the oxide, when under control; and to the study of the application of these techniques to FETs.

CRediT authorship contribution statement

Nil Solà-Peñafiel: Writing – original draft, Investigation, Data curation, Conceptualization. **Gema López-Rodriguez:** Writing – original draft, Investigation. **Pau Sindreu-Cladera:** Writing – original draft, Investigation. **Eric Navarrete:** Writing – original draft, Methodology, Investigation, Formal analysis. **Eduard Llobet:** Methodology, Investigation, Funding acquisition. **Juan Ramos-Castro:** Methodology, Investigation. **Isidro Martin:** Writing – original draft, Methodology, Investigation. **Xavier Manyosa:** Investigation. **Sandra Bermejo:** Methodology, Investigation. **Manuel Domínguez-Pumar:** Writing – original draft, Validation, Supervision, Methodology, Investigation, Funding acquisition, Formal analysis, Conceptualization.

Declaration of Competing Interest

The authors declare that they have no known competing financial interests or personal relationships that could have appeared to influence the work reported in this paper.

Acknowledgements

This work has been partially funded by MICINN, grants no. TED2021–131442B-C31, TED2021–131442B-C32, PID2020–115719RB-C21 (GETPV), TED2021–131778B (TROPIC) funded by MCIN/AEI/10.13039/5011000110033 / FEDER, UE and European Union "NextGenerationEU"/PRTR.; and by AGAUR, grant no. 56 30142 2021 2A. Activity financed through the Technology Transfer Operation 01.02.01 of the Rural Development Program of Catalonia 2014-2022

Appendix

A.1 First order vs second order sigma-delta experimental comparison

Closed-loop measurements were carried out using the first order sigma-delta modulator (see Figure A-1*)*.

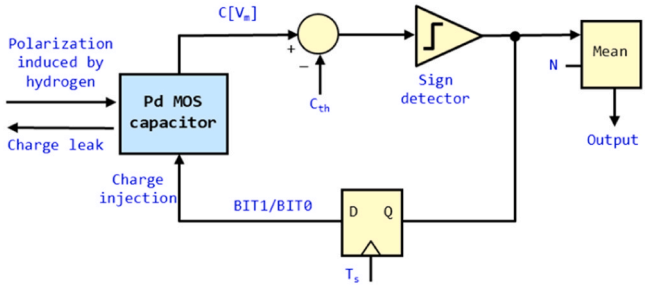

Figure A-1. First order sigma-delta control block diagram.

Figure A-2.A shows the measured capacitance (with and without window averaging) and the bitstream percentage (Figure A-2.C) as a function of time for an hydrogen pulse of 100 ppm for a first order sigma delta control. In the figure can be seen that this type of control is not able to keep the average capacitance constant at the chosen threshold capacitance (C_{th}), being slightly below when no hydrogen is applied and slightly above when the hydrogen pulse is applied. Moreover, in the bitstream percentage zoomed it can be seen that a plateau appears at 50 % (red circle in Figure A-3, left). This type of plateaus has been mentioned earlier and are a known first order sigma-delta modulator problem [33,41]. During the time intervals in which this occurs, which can last for several minutes, the output of the control is constant, a plateau, and thus the system is effectively in an open-loop configuration.

To improve the control performance, the device will be controlled using a second order sigma-delta modulator. With this control configuration, the average capacitance (Figure A-1.B) is almost constant around the threshold value and the Bitstream curve (Figure A-2.D and Figure A-3, right) does not show any plateaus. For this reason, all measurements in the experimental part have been carried out using a second order sigma-delta controller.

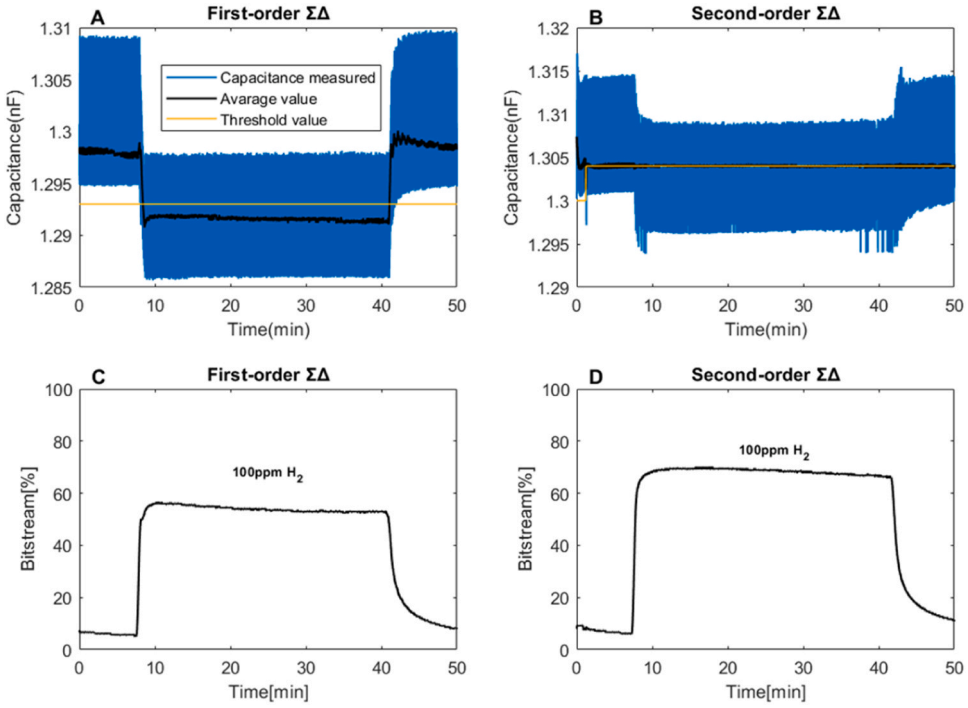

Figure A-2. Output comparison between first and second order sigma-delta control. A) Time evolution of the capacitance of the device, measured at V_{meas}, when controlled by a first order sigma-delta modulator. B) idem when controlled by a second order modulator. In both cases, the blue curve is the capacitance output, in black the same curve window-average by N = 50 samples. C) Filtered bitstream output of experiment in A). D) Filtered bitstream output of experiment in B). These measurements were performed at a constant flow rate of 80 mL/min. Closed-loop parameters: V_{low}= -6 V, V_{high}= -4 V, T_s= 0.15 s, T = 90°C.

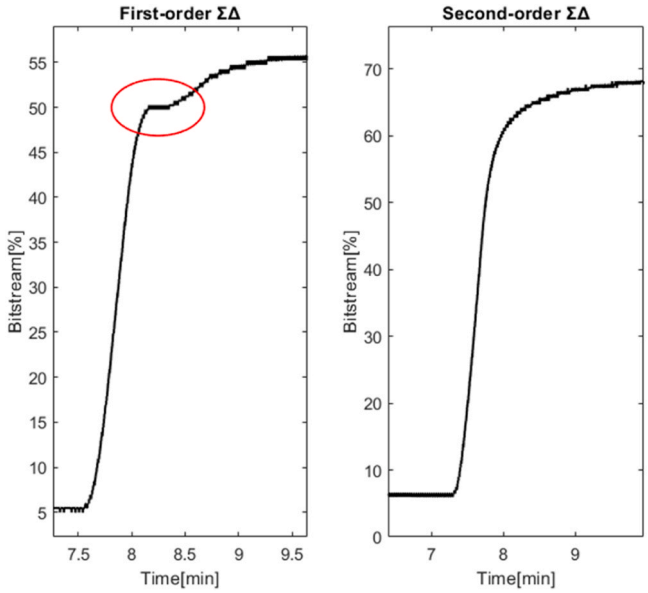

Figure A-3. Zoom in on the rise from 0 to 100 ppm in the experiment shown in Figure A.2, using a first-order sigma delta control (left) and a second-order sigma delta control (right). The red circle shows how the 50 % step slows down the response of the sensor. These measurements were performed at a constant flow rate of 80 mL/min. Closed-loop parameters: V_{low}= -6 V, V_{high}= -4 V, T_s= 0.15 s, T = 90°C.

Data availability

Data will be made available on request.

REFERENCES

[1] Alexandra M. OLIVEIRA, Rebecca R. BESWICK, Yushan YAN, A green hydrogen economy for a renewable energy society, Curr. Opin. Chem. Eng. 33 (2021) 100701.

[2] Selma ATILHAN, et al., Green hydrogen as an alternative fuel for the shipping industry, Curr. Opin. Chem. Eng. 31 (2021) 100668.

[3] I.I. CLARK, Woodrow W. RIFKIN, Jeremy. A green hydrogen economy, Energy Policy 34 (17) (2006) 2630–2639.

[4] D.A. Crowl, Y.D. Jo, The hazards and risks of hydrogen, J. Loss Prev. Process Ind. 20 (2) (2007) 158–164.

[5] T. Hübert, L. Boon-Brett, G. Black, U. Banach, Hydrogen sensors – A review, Sens. Actuators B: Chem. 157 (2) (2011) 329–352.

[6] I.I. Ivanov, A.M. Baranov, V.A. Talipov, S.M. Mironov, S. Akbari, I.V. Kolesnik, K. S. Napolskii, Investigation of catalytic hydrogen sensors with platinum group catalysts, Sens. Actuators, B 346 (2021) 130515.

[7] C. Wang, J. Yang, J. Li, C. Luo, X. Xu, F. Qian, Solid-state electrochemical hydrogen sensors: A review, Int. J. Hydrog. Energy 48 (80) (2023) 31377–31391.
[8] D. Berndt, J. Muggli, F. Wittwer, C. Langer, S. Heinrich, T. Knittel, R. Schreiner, MEMS-based thermal conductivity sensor for hydrogen gas detection in automotive applications, Sens. Actuators, A 305 (2020) 111670.
[9] Elsevier, 2022, September 15.
[10] M. Steele, B. MacIver, Palladium/cadmium-sulfide Schottky diodes for hydrogen detection, Appl. Phys. Lett. 28 (1976) 687–1687.
[11] Y.I. Chou, H.C. Chiang, C.C. Wang, Study on Pd functionalization of microcantilever for hydrogen detection promotion, Sens. Actuators B: Chem. 129 (2008) 72–78.
[12] Y.-n Zhang, M. Wang, N. Zhu, B. Han, Y. Liu, Optical fiber hydrogen sensor based on self-assembled PDMS/Pd-WO3 microbottle resonator, Sens. Actuators, B 375 (2023) 132866.
[13] X. Wang, L. Du, L. Cheng, S. Zhai, C. Zhang, W. Wang, G. Lei, Pd/Ni nanowire film coated SAW hydrogen sensor with fast response, Sens. Actuators, B 351 (2022) 130952.
[14] Constantinos Christofides, Andreas Mandelis, Solid-state sensors for trace hydrogen gas detection, 15 September, J. Appl. Phys. 68 (6) (1990) R1–R30.
[15] D. Gupta, D. Dutta, M. Kumar, P.B. Barman, C.K. Sarkar, S. Basu, S.K. Hazra, A low temperature hydrogen sensor based on palladium nanoparticles, Sens. Actuators B: Chem. 196 (2014) 215–222.
[16] C.C. Ndaya, N. Javahiraly, A. Brioude, Recent advances in palladium nanoparticles-based hydrogen sensors for leak detection, Sensors 19 (20) (2019) 4478.
[17] Julian W. Gardner, et al., CMOS Interfacing for Integrated Gas Sensors: A Review, IEEE Sens. J. 10 (12) (10 June 2010) 1833–1848.
[18] Ingemar Lundström, Hydrogen sensitive mos-s, tructures: Part 1: Princ. Appl." Sens. Actuators 1, 1 (Jan. 1981) 403–426.
[19] M. Armgarth, D. Söderberg, I. Lundström, Palladium and platinum gate metal-oxide-semiconductor capacitors in hydrogen and oxygen mixtures. Appl. Phys. Lett. 41 (7) (1982) 654–655.
[20] C. Nylander, M. Armgarth, C. Svensson, Hydrogen induced drift in palladium gate metal-oxide-semiconductor structures. J. Appl. Phys. 56 (4) (1984) 1177–1188.
[21] D. Dwivedi, R. Dwivedi, S.K. Srivastava, Sensing properties of palladium-gate MOS (Pd-MOS) hydrogen sensor-based on plasma grown silicon dioxide, Sens. Actuators B: Chem. 71 (3) (2000) 161–168.
[22] S.N. Rashkeev, D.M. Fleetwood, R.D. Schrimpf, S.T. Pantelides, Proton-induced defect generation at the Si-SiO/sub 2/ interface, IEEE Trans. Nucl. Sci. 48 (6) (2001) 2086–2092.
[23] N.S. Saks, D.B. Brown, Observation of H/sup + / motion during interface trap formation, IEEE Trans. Nucl. Sci. 37 (6) (1990) 1624–1631.
[24] J. Ding, E.X. Zhang, K. Li, X. Luo, M. Gorchichko, D.M. Fleetwood, Aging Effects and Latent Interface-Trap Buildup in MOS Transistors, IEEE Trans. Nucl. Sci. 68 (12) (2021) 2724–2735.
[25] T. Grasser, B. Stampfer, M. Waltl, G. Rzepa, K. Rupp, F. Schanovsky, B. Kaczer, Characterization and physical modeling of the temporal evolution of near-interfacial states resulting from NBTI/PBTI stress in nMOS/pMOS transistors. IEEE International Reliability Physics Symposium (IRPS), IEEE, 2018.
[26] T. Grasser, B. Kaczer, B. O'Sullivan, G. Rzepa, B. Stampfer, M. Waltl, The Mysterious Bipolar Bias Temperature Stress from the Perspective of Gate-Sided Hydrogen Release, IEEE Int. Reliab. Phys. Symp. . (IRPS) (2020).
[27] T. Grasser, W. Goes, Y. Wimmer, F. Schanovsky, G. Rzepa, M. Waltl, K. Rott, H. Reisinger, V. Afanas'ev, A. Stesmans, A. El-Sayed, A. Shluger, On the Microscopic Structure of Hole Traps in pMOS-FETs," in Proc. Intl, Electron Devices Meet. (IEDM) (Dec. 2014).
[28] A. El-Sayed, Y. Wimmer, W. Goes, T. Grasser, V. Afanas'ev, A. Shluger, "Theoretical Models of Hydrogen-Induced Defects in Amorphous Silicon Dioxide,", Phys. Rev. B 92 (11) (2015) 014107.
[29] W. Goes, Y. Wimmer, A.-M. El-Sayed, G. Rzepa, M. Jech, A. Shluger, T. Grasser, Identification of Oxide Defects in Semiconductor Devices: A Systematic Approach Linking DFT to Rate Equations and Experimental Evidence, Microelectron. Reliab. 82 (2018) 1–35.
[30] J. Stathis, E. Cartier, "Atomic Hydrogen Reactions with Pb Centers at the (100) Si/SiO2 Interface,", 601 (1–4), Phys. Rev. Lett. 92 (8) (2004) 087, 601 (1–4).
[31] David L.ópez Manuel Domínguez, Joan Pons-Nin David Molinero, "Dielectric charging control for electrostatic MEMS switches,", 5 May, Proc. SPIE 7679, Micro-Nanotechnol. Sens., Syst., Appl. II 76792J (2010), 5 May.
[32] E. Blokhina, et al., Dielectric Charge Control in Electrostatic MEMS Positioners/Varactors, *J. Micro Syst.* 21 (3) (June 2012) 559–573.
[33] S. Gorreta, J. Pons-Nin, E. Blokhina, O. Feely, M. Domínguez-Pumar, Delta-Sigma Control of Dielectric Charge for Contactless Capacitive MEMS, *J. Micro Syst.* 23 (4) (Aug. 2014) 829–841.
[34] S. Gorreta, J. Pons-Nin, E. Blokhina, M. Dominguez, A Second-Order Delta-Sigma Control of Dielectric Charge for Contactless Capacitive MEMS, *J. Micro Syst.* 24 (2) (April 2015) 259–261.
[35] M. Domínguez-Pumar, C.R. Bheesayagari, S. Gorreta, G. López-Rodríguez, I. Martín, E. Blokhina, J. Pons-Nin, Charge Trapping Control in MOS Capacitors, IEEE Trans. Ind. Electron. 64 (4) (2016) 3023–3029.
[36] M. Dominguez-Pumar, C.R. Bheesayagari, S. Gorreta, G. Lopez-Rodriguez, J. Pons-Nin, Closed-Loop Compensation of Charge Trapping Induced by Ionizing Radiation in MOS Capacitors, IEEE Trans. Ind. Electron. 65 (3) (March 2018) 2518–2524.
[37] C. Bheesayagari, S. Gorreta, J. Pons-Nin, M. Domínguez-Pumar, Second order sigma-delta control of charge trapping for MOS capacitors, Microelectron. Reliab. 76 (2017) 635–639.
[38] M. Dominguez-Pumar, S. Gorreta, J. Pons-Nin, F. Gomez-Rodriguez, D. M. Gonzalez-Castaño, M. Muschitiello, Closed-Loop Compensation of Dielectric Charge Induced by Ionizing Radiation, J. Micro Syst. 24 (3) (2015) 534–536.
[39] M. Domínguez-Pumar, S. Gorreta, J. Pons-Nin, F. Gómez-Rodríguez, D. M. González-Castaño, Charge induced by ionizing radiation understood as a disturbance in a sliding mode control of dielectric charge, Microelectron. Reliab. 55 (9) (2015) 1926–1931.
[40] M. Domínguez-Pumar, M. de la Torre Juárez, S. Navarro, M. Marin, J. Gómez-Elvira, C. Rosero-Pozo, J.A. Rodríguez-Manfredi, Dynamics of constant temperature anemometers for the Martian Atmosphere, Measurement 239 (2025) 115427.
[41] M. Domínguez-Pumar, E. Pérez, M. Ramón, V. Jiménez, S. Bermejo, J. Pons-Nin, Acceleration of the Measurement Time of Thermopiles Using Sigma-Delta Control, Sensors 19 (14) (2019) 3159.
[42] L. Kowalski, J. Pons-Nin, E. Navarrete, E. Llobet, M. Domínguez-Pumar, Using a Second Order Sigma-Delta Control to Improve the Performance of Metal-Oxide Gas Sensors, Sensors 18 (2018) 654.
[43] O. Feely, L.O. Chua, The effect of integrator leak in Σ-Δ modulation, IEEE Trans. Circuits Syst. I 38 (1991) 1293–1305.
[44] G. Zheng, E.I. Altman, The oxidation of Pd(111), Surf. Sci. 462 (1–3) (2000) 151–168.
[45] D. Zhang, C. Jin, H. Tian, Y. Xiong, H. Zhang, P. Qiao, J. Fan, Z. Zhang, Z.Y. Li, J. Li, An in situ TEM study of the surface oxidation of palladium nanocrystals assisted by electron irradiation, Nanoscale 9 (19) (2017) 6327–6333.

Nil Solà-Peñafiel received the B.Sc. degree in Electronic Engineering for Telecomunications and the M.Sc. degree in Electronic Engineering from the Universitat Politècnica de Catalunya (UPC) and the Universitat Oberta de Catalunya (UOC), in 2021 and 2024 respectively. He is currently a research assistant at the Micro and Nano Technologies group, Electronic Engineering department of UPC. His research interests include sensors for space application, closed-loop control systems, sigma-delta modulators, and MEMS sensors and actuators.

Gema López (UPC, Assistant professor). She obtained her degree in Electronic engineering (UPC) in 2005, and her Ph.D. in Electronic Engineering (UPC) in 2016. She has been working for more than 15 years developing and fabricating microelectronic devices in a cleanroom environment at the facilities of the Electronic Department (UPC). She has participated in the fabrication of the wind sensor of the MEDA instrument for NASA mission Mars2020. She has also collaborated with INTA and Solar MEMS company in the fabrication of a solar sensor for space applications (NANOSAT1B). Currently, the solar sensor is on board dozens nanosatellites. She combines the fabrications of devices oriented to space applications with the fabrication and characterization of other microelectronics devices like high efficiency solar cells. Author of 22 JCR papers, 17 international conference journal works.

Pau Sindreu-Cladera received the Engineering Physics degree from the Universitat Politècnica de Catalunya (UPC), Barcelona, Spain, in 2023. He is currently a research assistant in the Space Science and Technology (CTE-CRAE) of the Institute of Space Sciences of Catalonia (IEEC), in collaboration with the Micro and Nano Technologies Research Group of the UPC. His research interests include control and interface electronics for sensors and MEMS, as well as simulations, for space-related and chemical applications.

Eric Navarrete received his bachelor's in Chemistry and his master's in Nanoscience and Nanotechnology from University Rovira i Virgili and Northeastern University, Boston. He obtained his PhD. on technologies for Nanosystems in 2021 at University Rovira i Virgili. He worked under several projects to synthetize new nanomaterials and stayed for 3 months in Kyushu University, Japan. In 2020 under the LLAVOR project he obtained a Post-graduate title by UPF-BMS to bring the technology from the laboratory to the market starting its innovation and entrepreneurship career. Currently, he is also involved in the gas sensing Start-up NanoChronia as a co-founder and CTO.

Eduard Llobet is a full professor at the Department of Electronic Engineering of the Universitat Rovira i Virgili in Tarragona (Spain). He was awarded a Ph.D. in 1997 from the Technical University of Catalonia (Barcelona). He is an expert in Gas sensors, low-dimensional metal oxides, MEMS, and flexible platforms.

Juan Ramos-Castro received the Telecomunication Engineering and Eng.D degrees from the Universidad Politècnica de Catalunya (UPC), Barcelona, Spain, in 1992 and 1997, respectively. In 1992, he joined the Electronic Engineering Department, as a Lecturer and, since 1997, he has been an Associate Professor, teaching courses in several areas of electronic instrumentation. He is member of the board of directors of the Institute of Space Studies of Catalonia (IEEC). His research areas of interests are on the design of ultra low noise measurement systems with applications into the biomedical and space instrumentation fields.

Isidro Martín received the M.Sc. and Ph.D. degrees in ingeniería de telecomunicación from the Universitat Politècnica de Catalunya, Barcelona, Spain, in 1999 and 2004, respectively. He is an associate professor at UPC since 2008. His research interest has been always related to photovoltaic devices, in particular surface passivation. He developed high efficiency low temperature c-Si solar cells combining heterojunctions and laser processed contacts. He has also applied this technology to thin c-Si substrates. Recently, his activities are focused on c-Ge thermophotovoltaics devices where the IR photons emitted by a hot body are transformed to electrical energy.

Xavier Manyosa i Vilardell received his B.Sc. degree in Electronic Engineering for Telecommunications and his M.Sc. degree in Electronic Engineering from the Universitat Politècnica de Catalunya (UPC), Spain, in 2021 and 2023 respectively. He is currently a member of the Micro and Nano Technologies Research Group of the UPC as a Ph.D degree student. His research interests include sensors for space and planetary research applications, closed-loop control systems, and MEMS sensors and actuators.

Sandra Bermejo (UPC, Full Professor) earned the M.Sc. in Electrical Engineering and the Ph.D. degree in 2000 and 2004 respectively. Between 2015 and 2023, she served as the Vice Dean of the Barcelona School of Telecommunication Engineering (ETSETB) at the Universitat Politècnica de Catalunya (UPC). Her research endeavors are centered within the Micro and Nanotechnologies research group at UPC, where she leads the electrokinetics line. Her research objectives primarily revolve around the advancement of technology tailored for the production of functional nano-devices, with applications spanning the domains of photonics, energy, and sensing. The group has the achievement of developing a pioneering supercapacitor for energy harvesting, fully engineered with dielectric nanoparticles. She has actively contributed to a total of 29 competitive research projects, both at the national and European levels, leading 4 of them. She has managed 4 technology transfer projects with IT companies and research centers. She is author of more than 50 international journal papers and book chapters, more than 60 conference contributions and holds 3 patents.

Manuel Domínguez-Pumar (UPC-IEEC, Full Professor) He has been working in the field of sensors for more than 25 years. He contributed to the technology used in the Martian wind sensors of three NASA missions: REMS (MSL), TWINS (InSight) and MEDA (Mars2020), from the beginning. He was awarded a NASA group award: MSL REMS Instr. Development and Science Team in 2013. He is expert in sensors for planetary exploration, gas sensors and nonlinear control. He is also involved in the gas sensing Start-up NanoChronia as a co-founder.